Multivalued mappings in generalized chaos synchronization

Nikolai F. Rulkov,[1] Valentin S. Afraimovich,[2] Clifford Tureman Lewis,[1,3] Jean-Rene Chazottes,[2,4] and Albert Cordonet[2,5]
[1]*Institute for Nonlinear Science, University of California, San Diego, La Jolla, California 92093-0402*
[2]*IICO-UASLP, Avenida Obregón 64, 78000 San Luis Potosí, SLP, México*
[3]*Department of Physics, University of California, San Diego, La Jolla, California 92093*
[4]*IME-USP, Rua do Matão, 1010, 05508-900 São Paulo, Brazil*
[5]*Centre de Physique Théorique, Université de la Méditerranée, Luminy Case 907, F-13288 Marseille Cedex 9, France*
(Received 19 December 2000; published 22 June 2001)

The onset of generalized synchronization of chaos in directionally coupled systems corresponds to the formation of a continuous mapping that enables one to persistently define the state of the response system from the trajectory of the drive system. A recently developed theory of generalized synchronization of chaos deals only with the case where this synchronization mapping is a single-valued function. In this paper, we explore generalized synchronization in a regime where the synchronization mapping can become a multivalued function. Specifically, we study the properties of the multivalued mapping that occurs between the drive and response systems when the systems are synchronized with a frequency ratio other than one-to-one, and address the issues of the existence and continuity of such mappings. The basic theoretical framework underlying the considered synchronization regimes is then developed.

DOI: 10.1103/PhysRevE.64.016217 PACS number(s): 05.45.Xt, 47.52.+j, 82.40.Bj

I. INTRODUCTION

The synchronization of oscillations is one of the most interesting nonlinear phenomena and is an inherent part of many processes studied in a wide range of natural systems, including such diverse areas as neurobiological networks and solitary systems. As a result, the corresponding theory is extensively utilized in many practical applications [1–3]. The dynamical theory of the synchronization of periodic oscillations, which relates the onset of synchronization to the birth of a stable limit cycle due to the bifurcation of the motion on a two-dimensional ergodic torus, is due to Van der Pol [4]. Since the discovery of chaotic behavior in nonlinear oscillators and the ability of chaotic oscillators to synchronize, the framework of the dynamical theory of synchronization has been significantly modified. The theory now encompasses the major properties inherent in the synchronization that deal with limiting sets (called chaotic attractors) that are dynamically much richer than isolated limit cycles [5].

Different notions of synchronization occurring in chaotic oscillators have been introduced in order to explore the qualitative dynamical changes caused by the onset of chaos synchronization in numerous experimental studies. Such notions include the cases of *identical* synchronization, where identical chaotic oscillations are usually studied in coupled systems with identical individual dynamics [6,7], *generalized* synchronization, which extends the notion of identical synchronization to cases of directionally coupled systems with nonidentical individual dynamics [5,8–11], and *phase* synchronization that usually deals with the phase locking of the main frequencies in the spectrum of the chaotic systems while the chaotic components of the signals remain independent [12,13]. Studies of the phenomena of generalized and phase synchronization are largely motivated by the need for development of a theoretical framework that can be used to achieve a better understanding of synchronization in experiments with neurobiological systems where complex, chaotic behavior of neurons is very typical [11,14–16].

This paper addresses issues of generalized synchronization that arise in studies of chaos synchronization with a frequency ratio other than 1:1. As it is defined in [8], the onset of generalized synchronization in directionally coupled chaotic systems relates to the formation of a continuous mapping that transforms the trajectory on the attractor of the drive system into the trajectory of the response system. For systems with invertible dynamics, this is equivalent to the formation of a continuous mapping that links the current states of the systems once they settle down on the synchronous attractor. Since the introduction of the concept of generalized chaos synchronization, significant progress has been made in understanding the relationship between the properties of these synchronization mappings and the spectrum of Lyapunov exponents that characterize the synchronous chaotic attractor. A number of papers have analyzed conditions that guarantee the differentiability of the synchronization mapping, thus indicating the formation of a differentiable invariant manifold (in the joint phase space of the coupled systems) that contains the synchronized chaotic attractor (see, for example [17,18]). Simply put, this differentiability occurs when the rate of contraction in the direction transverse to the manifold is larger than the rate of contraction experienced by trajectories of the chaotic attractor in the direction tangent to the manifold. Such cases are distinguished as belonging to a subclass of generalized synchronization that has been named *differentiable generalized synchronization* [17].

The case of a nondifferentiable synchronization mapping formed in drive-response systems has been studied recently in [19]. In this paper, the stability of the response behavior in the whole phase space of the response system is linked with the existence of a mapping that maps the trajectories of the chaotic attractor in the driving system into the trajectories of the response system with a mapping that is a Hölder continuous function. These results help fill in the gap in parameter space that exists in between the synchronization regime where a smooth synchronization manifold exists and the

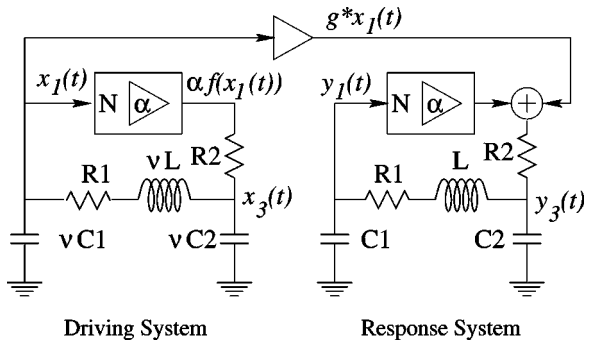

FIG. 1. The sketch of the circuit diagram for the experimental study of chaos synchronization with frequency ratio 2:1. The frequency ratio is controlled by the multiplier ν used to select the values of the inductors and capacitors in the drive and response circuits.

natural borders of the synchronization zones. In the present paper, we continue by studying how this theory of continuous functions can be extended to cases of chaos synchrony with frequency ratio other than 1:1, where the synchronization mapping can become multivalued.

In Sec. II, we present an example of chaos synchronization with frequency ratio 2:1 and study the formation of the multivalued mapping in detail. We do this by examining the bifurcations responsible for the transition from the single-valued mapping to the multivalued mapping as the regime of generalized synchronization of chaos changes. In Sec. III, in order to provide a more complete view of the synchronization mappings and their properties, we supplement our numerical simulation results with a discussion of some recent rigorous mathematical results not easily available to the reader, which are related to the considered regimes of generalized synchronization. We then review the results of the theory behind generalized synchronization with continuous functions and develop a similar theory for the case of multivalued functions.

II. CHAOS SYNCHRONIZATION WITH FREQUENCY RATIO 2:1

We consider a regime of chaos synchronization with frequency ratio 2:1. This type of synchronization was earlier observed in the experiments with two directionally coupled chaotic circuits. The sketch of the experimental setup is presented in Fig. 1. The details of the experiment and the parameters of the circuits can be found in [20].

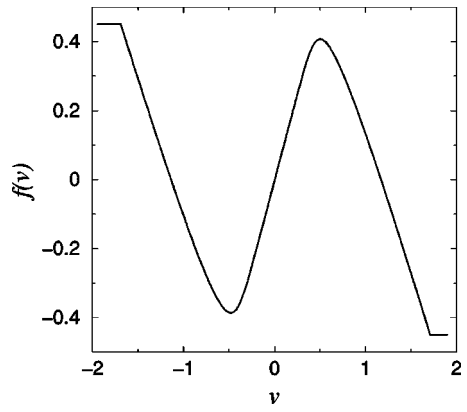

FIG. 2. The shape of the nonlinear function $f(\ )$ measured in the experimental setup.

In this paper we present a detailed analysis of this synchronization regime based on numerical simulation results.

A. Model

The dynamics of the drive circuit are described by the set of differential equations of the form [21]

$$\begin{aligned} \nu\dot{x}_1 &= x_2 \\ \nu\dot{x}_2 &= -x_1 - \delta x_2 + x_3 \\ \nu\dot{x}_3 &= \gamma(\alpha_1 f(x_1) - x_3) - \sigma x_2 . \end{aligned} \tag{1}$$

The response system equations are

$$\begin{aligned} \dot{y}_1 &= y_2 \\ \dot{y}_2 &= -y_1 - \delta y_2 + y_3 \\ \dot{y}_3 &= \gamma(\alpha_2 f(y_1) - y_3 + g x_1) - \sigma y_2 , \end{aligned} \tag{2}$$

where $\gamma = \sqrt{LC_1}/R_2C_2 = 0.294$, $\sigma = C_1/C_2 = 1.52$, $\delta = R_1\sqrt{C_1/L} = 0.534$, $\alpha_1 = 15.93$ and $\alpha_2 = 16.7$ are the fixed system parameters and g is the coupling strength. Variables x_1, x_3, y_1, and y_3 correspond to the voltages across the capacitors (see Fig. 1). Variables x_2 and y_2 are proportional to the current through the inductors in the drive and response circuits, respectively. The nonlinear function $f(\ )$ models the input-output characteristics of a nonlinear converter (N) used in the circuit. The shape of the nonlinearity is presented in Fig. 2. In the numerical simulation, we modeled the function $f(\ )$ with the formulas

$$f(x) = \mathrm{sgn}(x)(a - \sqrt{d(f_p(x) - a)^2 + c})/d,$$

where

$$f_p(x) = \begin{cases} |x| & \text{if } |x| \le a \\ -q(|x| - p) & \text{if } a < |x| \le b \\ -a & \text{if } |x| > b, \end{cases}$$

$d = (a^2 - c)/a^2$, $q = 2a/(b-a)$, $p = (b+a)/2$. The values of the parameters a, b, and c are chosen to be equal to 0.5, 1.8, and 0.03, respectively (see [21] for details). The parameter ν in the equations of the drive system is the time scaling parameter, which is used to select the frequency ratio of the synchronization zone.

The chaotic attractors occurring in the uncoupled drive and response systems with these parameter settings are shown in Fig. 3. Since we are interested in studying the chaos synchronization regime with a frequency ratio of 2:1, the parameter ν was set equal to 0.498. As a result, the phase

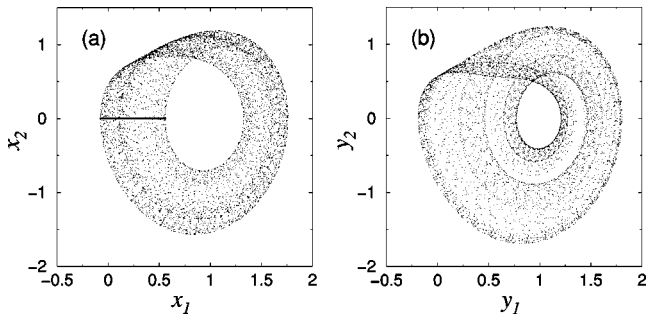

FIG. 3. Chaotic attractors of the drive system computed with the parameter value $\alpha_1=15.93$ (a), and the uncoupled response system (b). The bold dots on the trajectories of the driving attractor show the points where the chaotic trajectories cross the Poincaré cross section ($x_2=0$ with $dx_2/dt>0$).

velocity of the trajectories of the driving attractor is about twice as high as that of the response attractor.

B. Onset of generalized synchronization

Introduction of sufficiently strong coupling between the systems results in the onset of synchronization. The regime of synchronization that occurs when $g=2.5$ is presented in Fig. 4. The onset of synchronization in this case is detected using Lissajous figures, by observing the attractors in the Poincaré cross section, and by utilizing the auxiliary system method. Each of these methods will be briefly explained in the following paragraphs.

The Lissajous figure is a standard approach frequently utilized in traditional studies of synchronization between periodic oscillators. It enables one to clearly see the onset of phase locking and define the frequency ratio of the particular synchronization zone. For the frequency ratio 2:1, the Lissajous figure has a form similar to the shape of the digit ''8.'' Despite the fact that due to the chaotic behavior the Lissajous figure does not appear as a closed curve, it is still not difficult to see the onset of phase locking and identify the

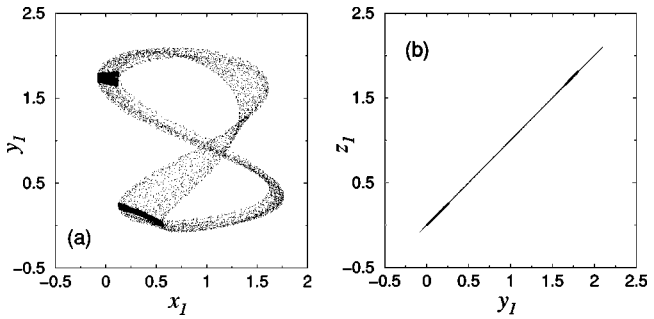

FIG. 4. (a) The Lissajous figure for the synchronized chaotic oscillations plotted on the plane of variables from the drive and response (x_1,y_1), and (b) the projections of the corresponding chaotic trajectories onto the plane of similar variables in the response and auxiliary systems (y_1,z_1). The strength of the coupling is $g=2.5$. The bold dots show the points on the chaotic trajectories corresponding to the moments of time when the trajectory of the drive system crosses the Poincaré cross section $(x_2=0)$ with a positive value of dx_2/dt .

frequency ratio [see Fig. 4(a)].

Analysis of generalized synchronization of chaos with the help of Poincaré cross sections was proposed in [22]. In this analysis, we define the Poincaré cross section in the drive system and detect the moments of time when driving trajectory crosses it. At these moments, we sample the state of the response system and compare the points to the corresponding set of the points in the drive system. This method simplifies the analysis of chaotic attractors by reducing their dimension by one. It helps to detect the onset of phase locking and, in some cases, to examine the onset of topological equivalence between the attractors in the synchronized drive and response systems. In the numerical simulations we analyze the properties of the chaotic attractors on the Poincaré cross section $(x_2=0)$ by computing the points where the trajectories cross the value $x_2=0$ with positive values of dx_2/dt [see Fig. 3(a)].

The auxiliary system method was proposed as a practical method of detecting the formation of a continuous mapping through the ability of persistently pointing out the current state of the response system without direct computation of the map [23]. This method assumes the use of a third (auxiliary) system that is an exact replica of the response system. In our case, the auxiliary system is of the form

$$\begin{aligned} \dot{z}_1 &= z_2 \\ \dot{z}_2 &= -z_1-\delta z_2+z_3 \\ \dot{z}_3 &= \gamma(\alpha_2 f(z_1)-z_3+gx_1)-\sigma z_2 . \end{aligned} \tag{3}$$

Due to the identity of the dynamics of the response and auxiliary systems, the nine-dimensional space encompassing all three coupled systems has an invariant manifold $\mathbf{y}=\mathbf{z}$, where $\mathbf{y}$ and $\mathbf{z}$ are vectors of the variables in the response and auxiliary systems, respectively. When this manifold contains the entire chaotic attractor, a continuous mapping exists that projects the trajectories of the drive system onto the trajectories of the response systems after transients die out (see [23] for details). Therefore, the formation of a chaotic attractor in the invariant manifold $(\mathbf{y}=\mathbf{z})$ constitutes the onset of generalized synchronization between the drive and response systems. Such a chaotic attractor occurs in our simulation with $g=2.5$ [see Fig. 4(b)].

When one utilizes this method in numerical simulations, it can be difficult to ensure that the chaotic set of trajectories in the invariant manifold does not contain transversely unstable limit sets. Due to the identity of the response and auxiliary systems and the limited accuracy of numerical simulations, the chaotic trajectory can settle down on the invariant manifold $\mathbf{y}=\mathbf{z}$, even if the chaotic set in the manifold contains transversely unstable limiting subsets. This artifact of numerical simulation can be resolved by breaking the symmetry between the response and auxiliary systems. In our simulations, we accomplish this by using slightly different values of coupling. The coupling of the auxiliary system is larger than the value of coupling in the response system by a value of $\Delta g=0.01$, less than 1% of the coupling strength used.

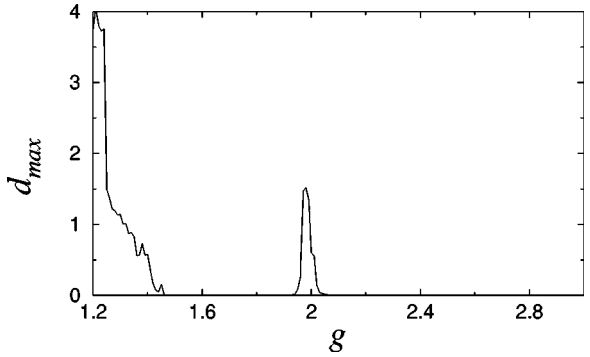

FIG. 5. The maximal deviation between the states of the response and auxiliary systems versus the value of coupling parameter g computed with $\Delta g = 0.01$.

C. Two regimes of generalized synchronization

The goal of this section is to examine in detail the main features of two qualitatively distinct regimes of generalized synchronization observed for different values of coupling in some previous experimental studies of chaos synchronization with a frequency ratio of 2:1 (see [20] for details on the experimental setup). In order to point out the change between the regimes of generalized synchronization versus variation of the coupling parameter, we analyzed the g dependence of $d_{max}(g) = \{\sqrt{(\mathbf{z}-\mathbf{y})^T(\mathbf{z}-\mathbf{y})}\}_{max}$, which is the maximal deviation between the response and auxiliary systems computed for the chaotic trajectories after transients die out. This dependence is presented in Fig. 5. Synchronization takes place for values of g where $d_{max}(g)$ is approximately equal to zero. In Fig. 5 there are two intervals of g that correspond to two synchronization regimes. These intervals are separated by a region of asynchronous behavior appearing around $g = 2.0$.

The oscillations occurring in the synchronization interval $g > 2.1$ correspond to the chaotic attractor shown in Fig. 4. When the value of coupling decreases and arrives at the border of this synchronization interval, generalized synchronization terminates. The chaotic attractor corresponding to these asynchronous oscillations, computed for $g = 2.0$, is presented in Fig. 6. The destruction of the generalized synchronization follows from the appearance of sporadic outbursts of nonidentical behavior in the response and auxiliary systems, which are seen in Fig. 6(b). Such outbursts are indicative of the existence of transversely unstable limiting trajectories in the chaotic set located in the manifold $\mathbf{y} = \mathbf{z}$ and therefore, indicates the inclusion of conditionally unstable limiting trajectories in the chaotic attractor residing in the phase space of the drive and response systems.

Further decrease of the coupling strength again results in the onset of synchronization when the value of coupling is in the second interval of synchronization that takes place between $g \approx 1.5$ and $g \approx 1.9$ (see Fig. 5). The synchronized chaotic attractor that occurs in this case is shown in Fig. 7. In the joint phase space of the drive and response systems this attractor represents a closed ribbon formed after a ''period doubling'' of the synchronized chaotic attractor studied in the first interval of synchronization, compare Figs. 4(a) and 7(a). Due to the period doubling that occurs in the response system (the driving system remains unchanged), the synchronization mapping for this attractor becomes a one-to-two mapping. Depending on initial conditions, the synchronized response oscillations settle down on the ribbon with one of two different phases. As a result, the single synchronized attractor in the drive-response system is presented as two different attractors in the drive-response-auxiliary system, one in the synchronization manifold $\mathbf{y} = \mathbf{z}$ and the other one outside the manifold [see Fig. 7(b)].

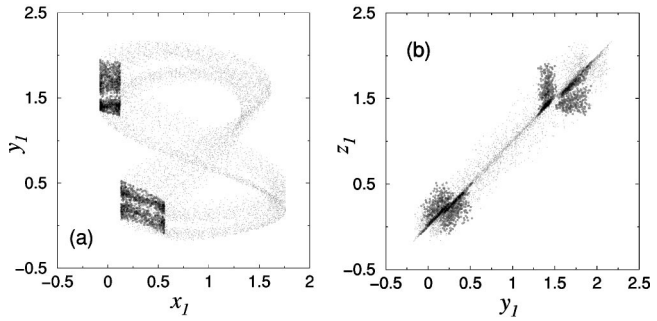

FIG. 6. The regime of asynchronous chaotic oscillations computed for $g = 2.0$. (a) The Lissajous figure in the plane (x_1, y_1), and (b) the projections of the corresponding chaotic trajectories onto the plane (y_1, z_1). The bold dots show the points on the chaotic trajectories corresponding to the moments of time when the trajectory of the drive system crosses the Poincaré cross section $(x_2 = 0)$ with a positive value of dx_2/dt.

In order to examine the synchronous chaotic attractors in more detail and to understand the properties of the corresponding synchronization mappings, we study the location and stability of the limiting sets contained in the attractors. These limiting sets are the unstable periodic orbits (UPOs) embedded in the chaotic attractor.

D. UPOs and the synchronization mappings

It is well known that phase locking of the unstable periodic orbits in the coupled chaotic systems plays a significant

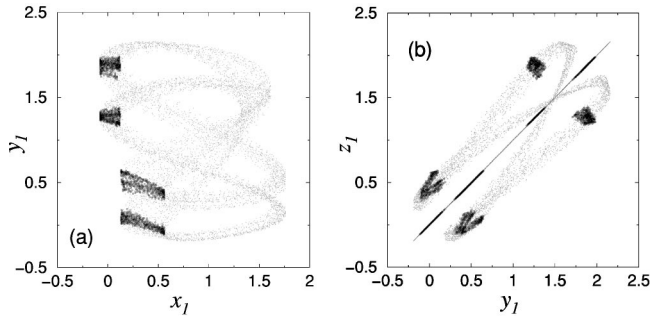

FIG. 7. The regime of synchronized chaotic oscillations computed for $g = 1.8$. (a) The Lissajous figure of the synchronized chaotic attractor in the plane of variables from the drive and response systems (x_1, y_1). (b) Two chaotic attractors corresponding to the synchronized chaos formed in the response and auxiliary systems plotted in the plane (y_1, z_1). The bold dots show the points on the chaotic trajectories corresponding to the moments of time when the trajectory of the drive system crosses the Poincaré cross section $(x_2 = 0)$ with a positive value of dx_2/dt.

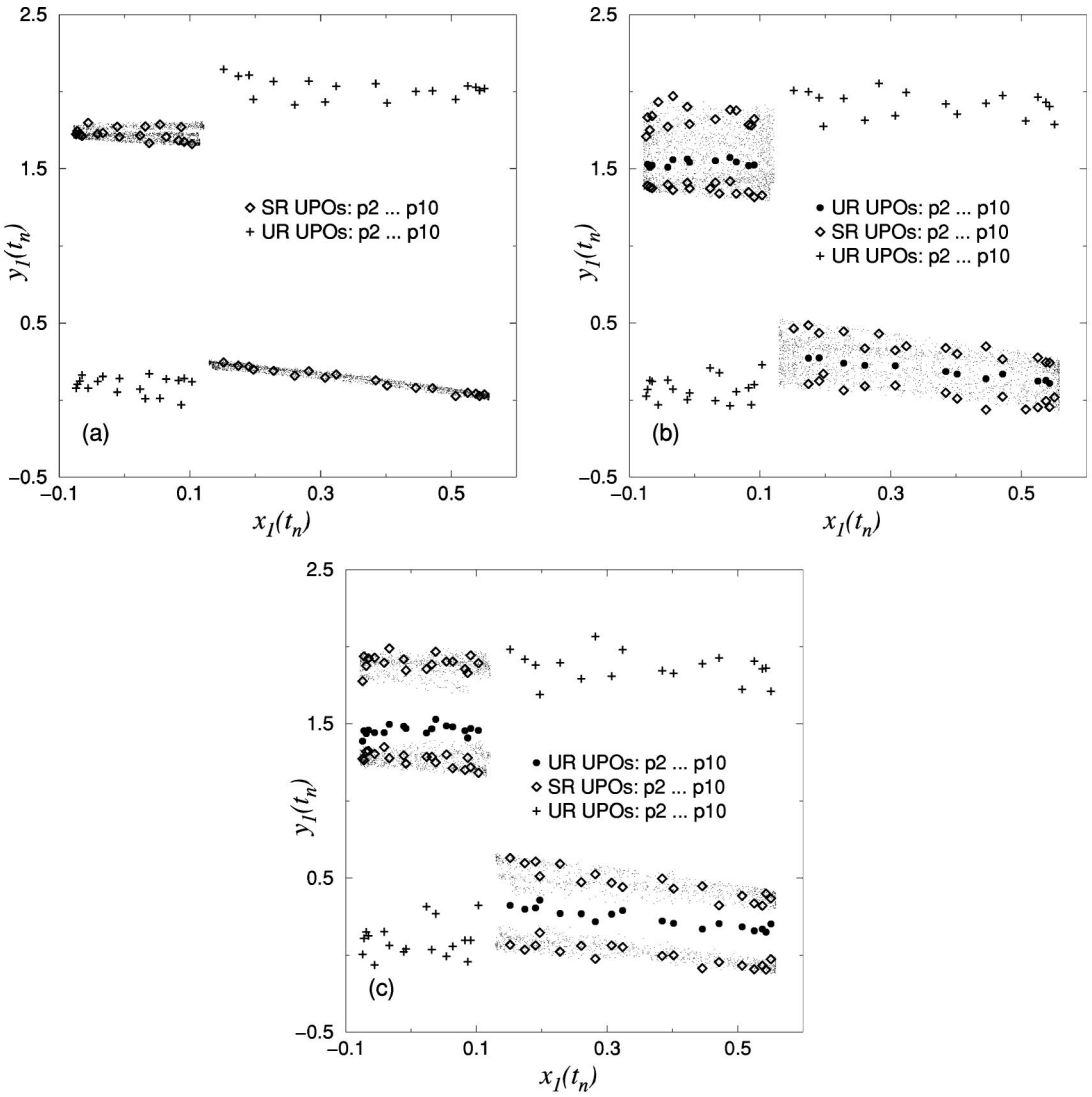

FIG. 8. The Poincaré cross sections of SR UPOs, UR UPOs and chaotic trajectories in the drive-response system computed for (a) $g=2.5$, (b) $g=2.0$, and (c) $g=1.8$.

role in the understanding of different regimes of chaos synchronization (see, for example [12,13,24–26]). Any UPO is characterized by the spectrum of multipliers μ_i or the corresponding Lyapunov exponents $\Lambda_i=\ln(\mu_i)/T_{UPO}$, where T_{UPO} is the period of the UPO. In the analysis of synchronization in directionally coupled systems, it is always useful to split the whole spectrum of Lyapunov exponents into two groups: the first is given by the dynamics of the autonomous drive system, and the second comes from the conditional dynamics of the response system. The conditional dynamics corresponds to the behavior induced in the response system by the driving signal.

Since the drive system is a three-dimensional dissipative system in the present case, the first group of the Lyapunov exponent spectrum for each UPO contains three exponents: $\Lambda_1>0$, $\Lambda_2=0$, and $\Lambda_3<0$. These exponents do not depend upon the coupling strength or any of the other parameters of the response system. The second group of exponents in the spectrum is due to the dynamics of the response system. Following [7] we call these exponents the *conditional Lyapunov exponents* Λ_i^c. If all of the conditional Lyapunov exponents of a UPO have negative values, we call that orbit a stable response (SR) UPO. If at least one conditional Lyapunov exponent of the UPO is positive, we call the orbit an unstable response (UR) UPO.

In our study, we consider all UPOs in the chaotic attractor of the driving system [shown in Fig. 3(a)] up to period 6, one of the period-8 UPOs, and one of the period-10 UPOs. Using the wave form of $x_1(t)$ of these orbits as a driving force, we computed the corresponding orbits that are formed in the driven response system. It is clear that, in this case, the stable periodic orbits correspond to the SR UPOs and the unstable ones to the UR UPOs formed in the joint phase space of the drive and response systems.

The results are shown in Fig. 8, where we plot the intersections of the UPOs with the Poincaré cross section ($x_2=0$, $dx_2/dt>0$) projected onto the variable plane (x_1,y_1). In order to see if the UPOs belong to the chaotic attractor we also plot, in the background, the points on the Poincaré cross section of the chaotic trajectory.

When the systems are synchronized with $g=2.5$, all the SR UPOs are inside the chaotic attractor, while the UR UPOs do not belong to the attractor, see Fig. 8(a). The trajectory of the synchronized chaotic attractor wanders around the SR UPOs that form the skeleton of the attractor. Since this skeleton does not contain UR UPOs, the response system always follows the driving chaotic trajectory in a stable manner. This fact explains the stability of the identical chaotic oscillations in the response and auxiliary systems [see Fig. 4(b)].

Decreasing the value of the coupling parameter g results in a sequence of bifurcations associated with the SR UPOs. These bifurcations create a large number of new UPOs, including new UR UPOs, which are added to the skeleton of the chaotic attractor [see Fig. 8(b) for the case $g=2.0$]. Since these new UR UPOs are inside the chaotic attractor they form regions where the response behavior for the chaotic driving is unstable. As a result, the synchronization is destroyed, see Fig. 6(b).

There is the coexistence of two types of UPOs that have different numbers of unstable directions in the chaotic attractor shown in Fig. 8(b). This is indicative of the onset of a nonhyperbolic situation [27–29]. Note that even though some kind of nonhyperbolic situation may exist in the chaotic attractor of the driving system, it does not make any impact on the response behavior and therefore, makes no impact on the synchronization between the drive and response systems. The synchronization is sensitive only to the nonhyperbolicity of the chaotic attractors contributed by the response system dynamics. This kind of nonhyperbolic situation is responsible for the inability to compute the trajectory of the response system if arbitrarily small perturbations of the system are taken into account [27]. This is the reason why the identical chaotic oscillations in the response and auxiliary systems do not follow the same path even when an arbitrary small perturbation is considered. It also directly indicates the destruction of the continuous synchronization mapping.

As one can see from Figs. 6(a) and 7(a), the further decrease of the coupling between the systems results in the period doubling of the ribbon formed by the chaotic attractor. When this period doubling ''bifurcation'' is complete, all the SR UPOs and the chaotic trajectories of the attractor are moved far enough from the region occupied by the UR UPOs and, as a result, all UR UPOs again reside only outside the chaotic attractor [see Fig. 8(c)]. This qualitative change of the chaotic behavior eliminates the nonhyperbolic situation caused by the dynamics of the response system and, as a result, the generalized synchronization is regained [see 7(b)]. It follows from the analysis of the SR UPOs that in this regime of chaos synchronization any point on the UPOs contained in the chaotic attractor of the driving system maps in to two points located on the corresponding SR UPOs. Therefore, this synchronization is characterized by one-to-two synchronization mapping.

In order to understand the properties of this synchronization mapping we studied the bifurcations of the SR UPOs when the value of coupling parameter is changed from high to low in the interval where the ribbon of the chaotic attractor experiences the period doubling bifurcation. This study, plotted in Fig. 9, reveals a very interesting fact. It turns out that not all the UPOs experience a period-doubling bifurcation in conjunction with the bifurcation of the ribbon. Indeed, the orbits that have a period, which is a multiple of 4 (the period of the chaotic ribbon after the bifurcation), are not subject to the period-doubling bifurcations [see Figs. 9(c) and 9(e)]. The other UPOs go through the period doubling bifurcation along with the ribbon.

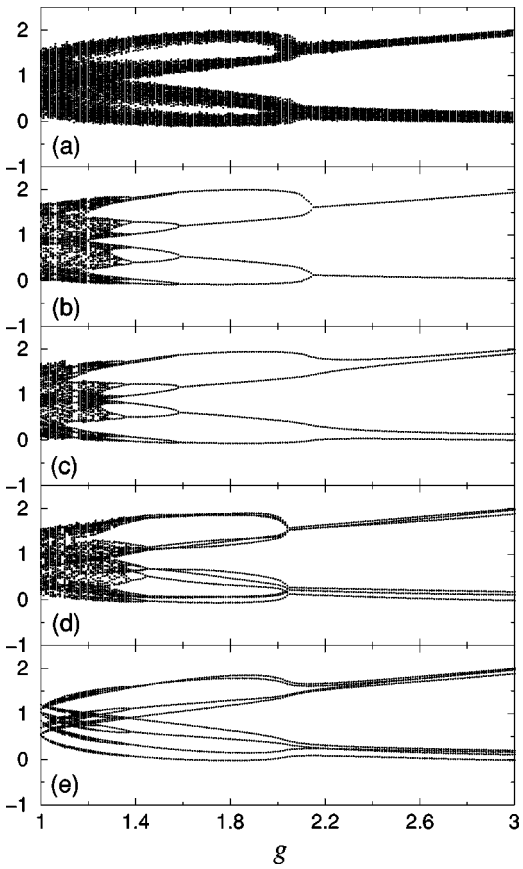

FIG. 9. The bifurcation diagram $y_1(t_n)$ vs g computed for the response system driven by (a) the chaos and by the UPOs: (b) $p2$, (c) $p4$, (d) $p6$, and (e) $p8$, which are found in the chaotic attractor of the driving system.

The difference in the bifurcation scenarios between the $p(4\times N)$ UPOs (with N an integer) and the other UPOs result in different synchronization mappings occurring when the response system is driven by these different UPOs. After the period doubling bifurcation, the orbits whose periods are not multiples of 4 have a one-to-two synchronization mapping [see Figs. 9(b) and 9(d)], while the $p(4\times N)$ orbits do not bifurcate and their synchronization mapping remains 1:1 [see Figs. 9(c) and 9(e)]. This situation raises the following question: How do these one-to-one synchronization mappings for the $p(4\times N)$ orbits fit into the one-to-two synchronization mapping that occurs for all trajectories of the chaotic attractor? The answer to this question comes from the analysis of the stable response images to periodic driving with the $p(4\times N)$ orbits. When the ribbon bifurcates, the $p(4\times N)$ orbits respond with the creation of a new pair of response orbits. One is SR UPO and the other is UR UPO

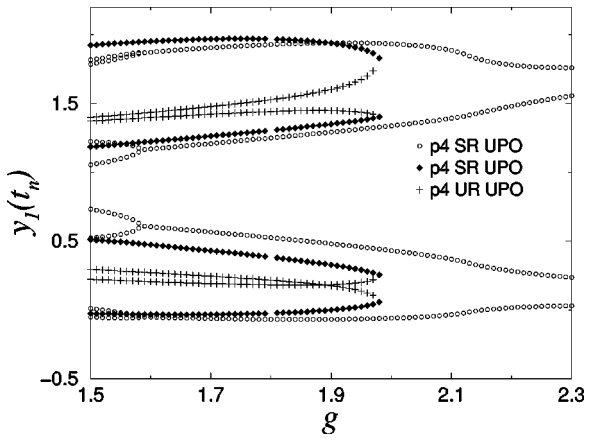

FIG. 10. The bifurcation diagram $y_1(t_n)$ vs g computed for the response system driven by the unstable periodic orbit $p4$ located in the chaotic attractor of the driving system. The stable response orbits are indicated by circles and diamonds. The unstable response orbit is indicated by crosses.

(this bifurcation scenario for the $p4$ orbit is presented in Fig. 10). Therefore, despite the fact that periodic synchronization for $p(4\times N)$ is characterized by a one-to-one mapping, each point on the $p(4\times N)$ orbit has two stable images in the phase space of the response system. Having two SR UPOs for each $p(4\times N)$ orbit, the orbits are able to conform to the one-to-two chaos synchronization mapping.

This example allows us to draw the following conclusions on the properties of generalized chaos synchronization with a multivalued mapping.

(1) The synchronized chaotic attractor represents a ribbon of chaotic trajectories that does not contain limiting sets with unstable response dynamics. Each point in the chaotic attractor of the driving system maps into M points in the chaotic attractor in the joint phase space of the drive-response system (in the presented example, $M=2$). The value of the number M is invariant over the attractor.

(2) These M points are located in the chaotic ribbon in such a way that they represent the different phases of the motion along the ribbon. Any trajectory of the synchronized attractor passes through all phases in sequential order. Therefore, the multivalued synchronization map can be presented as the cyclic sequence of the single-valued continuous maps.

(3) The UPOs of the chaotic attractor in the drive system have SR UPOs, each of which is characterized by the mapping where one point on the driving UPO maps into M points of the corresponding SR UPO. The exception to this rule includes only the UPOs of the driving chaotic attractor with periods that are multiples of the period of the chaotic ribbon. Each point on these special UPOs can map into a single point of the corresponding SR UPO. However, these UPOs should therefore have M stable response UPOs.

III. FUNCTIONS IN THE THEORY OF GENERALIZED SYNCHRONIZATION OF CHAOS

In this section we formulate the theoretical framework for the synchronization mappings that occur in those regimes of chaos synchronization similar to the one considered on the previous section. The main goal here is to link the properties of the synchronization mappings with the stability characteristics of the response system behavior.

As it was shown in the previous section, the use of a Poincaré cross section enables one to simplify the analysis of the synchronization mapping by studying the dynamics of the maps. In a rather general case, the maps occurring in the drive and response systems can be presented as maps with a skew product structure of the form

$$\mathbf{x}_{n+1}=\mathbf{F}(\mathbf{x}_n) \tag{4}$$

$$\mathbf{y}_{n+1}=\mathbf{G}_k(\mathbf{x}_n,\mathbf{y}_n), \tag{5}$$

where $\mathbf{x}$ and $\mathbf{y}$ are vectors consisting of the variables in the drive, response and auxiliary systems respectively, and k is a parameter depending on the strength of the coupling.

Since the first studies of chaos synchronization between *nonidentical* systems [5], synchronization was interpreted as the system behaving in such a way that for any orbit $(\mathbf{x}_n,\mathbf{y}_n)$, the coordinate $\mathbf{y}_n$ is just a function of the $\mathbf{x}_n$, once transients die out. The first rigorous results on generalized synchronization were obtained for cases where there exists a smooth manifold belonging to the graph of a function $\mathbf{y}=h(\mathbf{x})$ that is stable in the transversal direction and contains the chaotic attractor corresponding to the synchronized oscillations [17,18]. This approach relies on the theory of normally hyperbolic invariant manifolds.

In most studies of different regimes of generalized chaos synchronization, it is observed that in some region of k values, a function h seems to exist, but it is not smooth. As a result, the graph of h is a complicated geometrical object (see, for example [17,30]). In this section we discuss recent rigorous results on the properties of nonsmooth functions h and present new results for the case of multivalued mappings.

A. Results and examples concerning single-valued functions *h*

To make the paper self-contained, we first briefly discuss the rigorous results on the existence and continuity of the synchronization function h that were obtained in a previous work [19]. The paper demonstrates that the function h is Hölder continuous if the contraction rate in the response system is small and Lifschitz-continuous if it is greater than a critical value. Assume that $\mathbf{x}\in\mathbb{R}^m$ and $\mathbf{y}\in\mathbb{R}^n$, and that $\mathbf{G}_k$ is continuous and $\mathbf{F}$ is a homeomorphism (i.e., $\mathbf{F}$ is continuous and invertible with an inverse $\mathbf{F}^{-1}$ that is continuous). The dynamics in the joint phase space of the drive and response systems is determined by a map $\phi_k\colon (\mathbf{x}_n,\mathbf{y}_n)\mapsto(\mathbf{x}_{n+1},\mathbf{y}_{n+1})$. We also assume that in the joint phase space there exists a basin of attraction $B=B_{xy}\in\mathbb{R}^{m+n}$, i.e., $\phi_k(B)\subset \mathrm{Int}(B)$ for any $k\in S$, where S is a region in k space in which the systems (4) and (5) exhibit master-slave chaos synchronization. Without loss of generality, we assume that $B_{xy}=B_x\times B_y$, i.e., B_{xy} is a rectangle, where B_x (B_y) is a ball in $\mathbf{x}$ space ($\mathbf{y}$ space).

Denote by $\mathcal{A}_k$ the maximal attractor in B_{xy}, i.e., $\mathcal{A}_k=\cap_{n=0}^{\infty}\phi_k^n(B_{xy})$. Because of our assumptions,

$$\lim_{n\to\infty}|\mathbf{y}_n-\tilde{\mathbf{y}}_n|=0, \tag{6}$$

where $(\mathbf{x}_n,\mathbf{y}_n)=\phi_k^n(\mathbf{x}_0,\mathbf{y}_0)$, $(\mathbf{x}_n,\tilde{\mathbf{y}}_n)=\phi_k^n(\mathbf{x}_0,\tilde{\mathbf{y}}_0,)$ and $(\mathbf{x}_0,\mathbf{y}_0)$, $(\mathbf{x}_0,\tilde{\mathbf{y}}_0)$ are arbitrary points in B_{xy}.

To avoid nonessential technicalities it was supposed in [19] that the limit in Eq. (6) is achieved monotonically, i.e.,

$$|\mathbf{y}_{n+1}-\tilde{\mathbf{y}}_{n+1}|\leqslant|\mathbf{y}_n-\tilde{\mathbf{y}}_n| \tag{7}$$

for any $k\in S$ and any $n\geqslant 0$.

Let $\mathcal{A}_{k,x}:=\Pi_x\mathcal{A}_k$ be the image of $\mathcal{A}_k$ under the natural projection Π_x to $\mathbb{R}^m$.

Theorem 1A [19]. *(Existence)Under assumptions* (6) *and* (7)*, there exists a function* h: $\mathcal{A}_{k,x}\to\mathbb{R}^n$ *such that* $\mathcal{A}_k$ *is a graph of function* h.

We emphasize that it is the inversibility of **F** that ensures that h is a single-valued function. Continuity plays no role at this stage.

Theorem 2A [19]. *(Continuity) Under the assumptions of Theorem 1A, the function* h *is continuous.*

To obtain more detailed characteristics of this functional dependence, additional assumptions were made. It was assumed that

$$|\mathbf{y}_{n+1}-\tilde{\mathbf{y}}_{n+1}|\leqslant k_1|\mathbf{y}_n-\tilde{\mathbf{y}}_n| \tag{8}$$

where $k_1<1$. Of course, the parameter k_1 is a function of k. For the sake of simplicity, we assume that $k_1=k$. Thus,

$$|\mathbf{y}_{n+1}-\tilde{\mathbf{y}}_{n+1}|\leqslant k|\mathbf{y}_n-\tilde{\mathbf{y}}_n|,\quad 0<k<1. \tag{9}$$

It follows that

$$|\mathbf{G}_k(\mathbf{x},\mathbf{y})-\mathbf{G}_k(\mathbf{x},\tilde{\mathbf{y}})|\leqslant k|\mathbf{y}-\tilde{\mathbf{y}}| \tag{10}$$

for any $(\mathbf{x},\mathbf{y})$, $(\mathbf{x},\tilde{\mathbf{y}})\in B_{xy}$.

Assumption (9) implies that $|\mathbf{y}_n-\tilde{\mathbf{y}}_n|$ goes to zero exponentially fast, and this fact allows one to prove that h is Hölder continuous provided that the functions **F** and $\mathbf{G}_k$ have good smooth properties, or provided at the least that they are Lipschitz-continuous.

Considering the forward and backward dynamics of the driving system (4) we assume the following properties,

$$|\mathbf{F}(\mathbf{x})-\mathbf{F}(\tilde{\mathbf{x}})|\leqslant\gamma_+|\mathbf{x}-\tilde{\mathbf{x}}| \tag{11}$$

and

$$|\mathbf{F}^{-1}(\mathbf{x})-\mathbf{F}^{-1}(\tilde{\mathbf{x}})|\leqslant\gamma_-|\mathbf{x}-\tilde{\mathbf{x}}|, \tag{12}$$

where $\gamma_-,\gamma_+\geqslant 1$. When Lyapunov exponents do exist (when the dynamics are differentiable with additional suitable conditions), the quantities $\ln\gamma_+,\ln\gamma_-$ play the role of the forward and backward greatest Lyapunov exponents, respectively, and $\ln k$ plays the role of the conditional Lyapunov exponent.

It is assumed that function $\mathbf{G}_k(\mathbf{x},\mathbf{y})$ of the response system (5) is Lifschitz continuous with respect to **x**, i.e., for any $(\mathbf{x},\mathbf{y})$, $(\tilde{\mathbf{x}},\mathbf{y})\in B_{xy}$,

$$|\mathbf{G}_k(\mathbf{x},\mathbf{y})-\mathbf{G}_k(\tilde{\mathbf{x}},\mathbf{y})|\leqslant\eta|\mathbf{x}-\tilde{\mathbf{x}}| \tag{13}$$

where $\eta>0$.

Theorem 3A [19]. *(Hölder property) Under assumptions (10)–(13) the function* h *is Hölder continuous, i.e., for any* $0<\alpha<\alpha_c$*, and* $x,\tilde{x}\in\mathcal{A}_{k,x}$ *one has*

$$|h(\mathbf{x})-h(\tilde{\mathbf{x}})|\leqslant 2\rho|\mathbf{x}-\tilde{\mathbf{x}}|^\alpha, \tag{14}$$

where

$$\alpha\leqslant\alpha_c:=\frac{1}{1-\dfrac{\ln(\gamma_+\gamma_-)}{\ln k}}, \tag{15}$$

and $\rho\geqslant\rho_c$*, where* ρ_c *is the solution of the equation,*

$$\rho=\frac{\eta}{\gamma_+-k}\rho^{[\ln(\gamma_+\gamma_-)/\ln k]+1}\exp\left(\frac{\ln k-\ln|B_y|}{\ln k}\ln[\gamma_+\gamma_-]\right).$$

Theorem 4A [19]. *(Lipschitz property) Under the conditions of Theorem 3A and provided that*

$$0<k<\frac{1}{\gamma_-}, \tag{16}$$

the function h *is Lifschitz continuous, i.e.,*

$$|h(\mathbf{x})-h(\tilde{\mathbf{x}})|\leqslant L|\mathbf{x}-\tilde{\mathbf{x}}|, \tag{17}$$

where $L\geqslant L_c:=\eta\gamma_-/(1-k\gamma_-)$.

The considered theorems give a pretty clear picture of the complexity of the synchronization mappings that usually occur in different regimes of generalized synchronization of chaos. It follows from these results that even in the case of *differentiable generalized synchronization* [17], the change of the parameters toward the border of the synchronization zone will gradually reduce the rate of contraction in the response system. At some critical value of the contraction rate (see Theorems 3A and 4A), the smoothness of synchronization mapping will be destroyed while the systems remain synchronized with a nondifferentiable function.

Example: To illustrate the results above, let us consider coupled Hénon maps.

We consider the linear coupling of two *nonidentical* Hénon-type maps. For certain values of coupling strength, the hypotheses of our theorems are fulfilled.

Let f be the following invertible map: f: $[0,1]^2\to[0,1]^2$, $f(x_1,y_1)=(x_1',y_1')$ with

$$x_1'=y_1$$

$$y_1'=f_1(y_1)+bx_1$$

where f_1: $[0,1]\to[0,1]$ is Lipschitz, with Lipschitz constant γ_1, $0<b\leqslant 1$. Let f_1 be such that $f_1(y_1)\leqslant \gamma_1/2, \forall\ y_1 \in[0,1]$, and $(1+b_1)(\gamma_1/2)\leqslant 1$. The map f is a homeomorphism of the unit square. Let g_c be the following map: g_c: $[0,1]^4\to[0,1]^2$, $g_c(x_1,y_1,x_2,y_2)=(x_2',y_2')$ with

$$x_2'=y_2+c(y_1-y_2)$$

$$y_2'=f_2(y_2)+b_2x_2+c(f_1(y_1)+b_1x_1)-[f_2(y_2)+b_2x_2)],$$

where $0\leqslant c\leqslant 1$, f_2: $[0,1]\to[0,1]$ is Lipschitz, with Lipschitz constant γ_2, $(1+b_2)(\gamma_2/2)\leqslant 1$ and $f_2(y_2)\leqslant \gamma_2/2, \forall\ y_2\in[0,1]$. For convenience, we shall use the following shorthand: $v_1=(x_1,y_1)$ and $v_2=(x_2,y_2)$.

To have contraction in v_2 space, that is $|g_c(v_1,v_2)-g_c(v_1,\tilde{v}_2)|\leqslant k|v_2-\tilde{v}_2|$ with $0<k<1$, the following condition must be satisfied[1]:

$$c>1-\frac{1}{1+b_2+\frac{\gamma_2}{2}}.$$

The forward and backward expansion rates of **F** are, respectively, given by: $\gamma_+=1+\gamma_1/2$ and $\gamma_-=b_1^{-1}$.

Theorem 3A holds, i.e., the function h is Hölder continuous and one can easily check the following expression for the Hölder exponent,

$$\alpha_0=\frac{\ln\left[(1-c)\left(1+b_2+\frac{\gamma_2}{2}\right)\right]}{\ln\left(\frac{b_1(1-c)\left(1+b_2\frac{\gamma_2}{2}\right)}{1+\frac{\gamma_1}{2}}\right)}.$$

The condition (16) in Theorem 4A reads

$$c>1-\frac{b_1}{1+b_2+\frac{\gamma_2}{2}}.$$

According to Theorem 4A, this means that the function h is Lipschitz continuous.

B. Multivalued function *h*

The framework of chaos synchronization discussed above applies only to the cases when the function h is a single-valued function, because of the assumption (6). As a result this framework is not applicable to the case of synchronization presented in Fig. 7 where each point on the chaotic attractor $\mathcal{A}_{k,x}$ in driving system maps into two different points of the synchronized chaotic attractor $\mathcal{A}_k$. In this case B_y is not a simply connected region, and assumption (6) cannot be used. Below we reformulate the results on single-valued function in order to extend it to the case of multivalued function.

Assume that $B_y=\cup_{i=1}^p B_y^i$, where B_y^i are pairwise disjoint closed balls in the **y** space, B_x is a closed ball in the x space, and $B_{xy}=B_x\times B_y$.

We also assume that monotonic synchronization occurs in B_{xy}, i.e.,

$$\lim_{n\to\infty}|\mathbf{y}_n-\tilde{\mathbf{y}}_n|=0 \tag{18}$$

and

$$|\mathbf{y}_{n+1}-\tilde{\mathbf{y}}_{n+1}|\leqslant|\mathbf{y}_n-\tilde{\mathbf{y}}_n|, \tag{19}$$

where $(\mathbf{x}_n,\mathbf{y}_n)=\phi_k^n(\mathbf{x}_0,\mathbf{y}_0)$, $(\mathbf{x}_n,\tilde{\mathbf{y}}_n)=\phi_k^n(\mathbf{x}_0,\tilde{\mathbf{y}}_0,)$ and $(\mathbf{x}_0,\mathbf{y}_0)$, $(\mathbf{x}_0,\tilde{\mathbf{y}}_0)$ are arbitrary points in B such that $\mathbf{y}_0$ and $\tilde{\mathbf{y}}_0$ belong to the same ball B_y^i for some i.

Denote by $\mathcal{A}_k$ the maximal attractor in B_{xy}, i.e., $\mathcal{A}_k=\cap_{n=0}^{\infty}\phi_k^n(B_{xy})$ and let $\mathcal{A}_{k,x}:=\Pi_x\mathcal{A}_k$ be the image of $\mathcal{A}_k$ under the natural projection Π_x to $\mathbb{R}^m$.

In this situation some extensions of theorems 1A–4A hold.

Theorem 1B. (Existence) Under conditions (18) and (19), and provided that for any $\mathbf{x}\in\mathcal{A}_{k,x}$ *and for any* i, $1\leqslant i\leqslant p$, *there exist* $\mathbf{y}_i\in B_y^i$ *such that* $(\mathbf{x},\mathbf{y}_i)\in\mathcal{A}_k$, *there exist p functions* h_i: $\mathcal{A}_{k,x}\to\mathbb{R}^n$, $i=1,\ldots,p$ *such that graph* $(h_i)\subset B_x\times B_y^i$ *and* $\mathcal{A}_k=\cup_{i=1}^p$ *graph* (h_i).

Scheme of the proof. The proof is mainly the same as the one for single-valued case (Theorem 1A). However we need to emphasize the following facts. For any $\mathbf{x}\in\mathcal{A}_{k,x}$ and for any $n\geqslant 0$, the set $\phi_k^n(\mathbf{x},\cup_{i=1}^p B_y^i)$ has p connected components inside $(\mathbf{F}^n(\mathbf{x}),\cup_{i=1}^p B_y^i)$ and every set $(\mathbf{F}^n(\mathbf{x}),B_y^i)$ contains one and only one of them. Indeed, if we assume that $(\mathbf{F}^n(\mathbf{x}),B_y^i)$ contains more than one connected components for some i then it will imply that there exist a j such that $(\mathbf{F}^n(\mathbf{x}),B_y^j)$ contains no components. Since **F** is 1:1, it means that there are no points of the attractor in $(\mathbf{F}^n(\mathbf{x}),B_y^j)$ and we have a contradiction. From this point forward, one can follow the proof of Theorem 1A. □

Theorem 2B. (Continuity) Under assumptions of Theorem 1B, the functions h_i *are continuous, for* $i=1,\ldots,p$.

Scheme of the proof. Let $\mathbf{x}$ and $\tilde{\mathbf{x}}$ be close to each other and consider the points $(\mathbf{x},h_i(\mathbf{x}))$ and $(\tilde{\mathbf{x}},h_i(\tilde{\mathbf{x}}))$. We show now that $\phi_k^{-1}(\mathbf{x},h_i(\mathbf{x}))$ and $\phi_k^{-1}(\tilde{\mathbf{x}},h_i(\tilde{\mathbf{x}}))$ belong to the sets $(\mathbf{F}^{-1}(\mathbf{x}),B_y^j)$ and $(\mathbf{F}^{-1}(\tilde{\mathbf{x}}),B_y^j)$, respectively, with the same number j.

Assuming the contrary, i.e., $\phi_k^{-1}(\mathbf{x},h_i(\mathbf{x}))\in(\mathbf{F}^{-1}(\mathbf{x}),B_y^j)$ but $\phi_k^{-1}(\tilde{\mathbf{x}},h_i(\tilde{\mathbf{x}}))\in(\mathbf{F}^{-1}(\tilde{\mathbf{x}}),B_y^{j'})$ and $j'\neq j$. Therefore $\phi_k(\mathbf{F}^{-1}(\tilde{\mathbf{x}}),B_y^{j'})$ belongs to $(\tilde{\mathbf{x}},B_y^i)$ and $\phi_k(\mathbf{F}^{-1}(\tilde{\mathbf{x}}),B_y^j)$ belongs to $(\tilde{\mathbf{x}},B_y^{i'})$ where $i'\neq i$. Consider now the points $(\mathbf{F}^{-1}(\mathbf{x}),\mathbf{y})$ and $(\mathbf{F}^{-1}(\tilde{\mathbf{x}}),\mathbf{y})$, $\mathbf{y}\in B_y^i$. It follows that $\mathrm{dist}(\phi_k(\mathbf{F}^{-1}(\mathbf{x}),\mathbf{y}),\phi_k(\mathbf{F}^{-1}(\tilde{\mathbf{x}}),\mathbf{y}))$ is bounded from zero provided that $\mathbf{x}$ and $\tilde{\mathbf{x}}$ are close enough. Roughly speaking, this distance is greater than $\frac{1}{2}\mathrm{dist}(B_y^j,B_y^{j'})$. On the other side, we

[1]We use the norm $|v|=|x|+|y|$, where $v=(x,y)$.

know that $|\mathbf{F}^{-1}(\mathbf{x})-\mathbf{F}^{-1}(\tilde{\mathbf{x}})|$ is small, therefore by continuity of ϕ_k, dist$(\phi_k(\mathbf{F}^{-1}(\mathbf{x}),\mathbf{y}),\phi_k(\mathbf{F}^{-1}(\tilde{\mathbf{x}}),\mathbf{y}))$ is also small, resulting in a contradiction.

The rest of the proof is the same as in Theorem 2A. □

We assume now that conditions similar to Eqs. (8)–(13) hold in B_{xy}, i.e., inequalities (8)–(10) hold provided that $\mathbf{y}=\mathbf{y}_0$, $\tilde{\mathbf{y}}=\tilde{\mathbf{y}}_0$ belong to the same connected component in the set B_y; other conditions remain the same.

Taking into account the schemes of the proofs of Theorems 1B and 2B, one can check that the proofs of the following two theorems are similar to the proofs of Theorems 3A and 4A.

Theorem 3B. (Hölder property) If the conditions are satisfied, under assumptions of Theorem 1B, the functions h_i, $i=1,\ldots,p$ *are Hölder continuous, i.e., for any* $0<\alpha<\alpha_c$, $\mathbf{x},\tilde{\mathbf{x}}\in\mathcal{A}_{k,x}$ *one has,*

$$|h_i(\mathbf{x})-h_i(\tilde{\mathbf{x}})|\leqslant 2\rho|\mathbf{x}-\tilde{\mathbf{x}}|^{\alpha}, \tag{20}$$

where

$$\alpha\leqslant\alpha_c:=\frac{1}{1-\dfrac{\ln(\gamma_+\gamma_-)}{\ln k}}, \tag{21}$$

and $\rho\geqslant\rho_c$, *where* ρ_c *is the solution of the equation,*

$$\rho=\frac{\eta}{\gamma_+-k}\rho^{[\ln(\gamma_+\gamma_-)/\ln k]+1}\exp[\Delta(k,\gamma_+,\gamma_-)], \tag{22}$$

where

$$\Delta(k,\gamma_+,\gamma_-):=\frac{\ln k-\ln(\max_i|B_y^i|)}{\ln k}\ln(\gamma_+\gamma_-). \tag{23}$$

Theorem 4B. (Lipschitz property) Under conditions of Theorem 3B and provided that

$$0<k<\frac{1}{\gamma_-}, \tag{24}$$

the functions h_i, $i=1,\ldots,p$, *are Lipschitz-continuous, i.e.,*

$$|h_i(\mathbf{x})-h_i(\tilde{\mathbf{x}})|\leqslant L|\mathbf{x}-\tilde{\mathbf{x}}|, \tag{25}$$

where $L\geqslant L_c:=\eta\gamma_-/1-k\gamma_-$.

In order to deal with problems in the case of multivalued function h we make use of the auxiliary systems approach [23]. Consider an auxiliary system that is a replica of the response system (5) and given by the equation of the form

$$\mathbf{z}_{n+1}=\mathbf{G}_k(\mathbf{x}_n,\mathbf{z}_n). \tag{26}$$

Note that the auxiliary system (26) can serve, as well as in the case of standard generalized synchronization, to indicate the validity of synchronization.

Let the dynamics in the joint phase space of the drive, response and auxiliary systems be determined by a map ψ_k: $(\mathbf{x}_n,\mathbf{y}_n,\mathbf{z}_n)\mapsto(\mathbf{x}_{n+1},\mathbf{y}_{n+1},\mathbf{z}_{n+1})$. Due to the identity between the response and auxiliary system there always exist an invariant manifold M_S: $\mathbf{y}=\mathbf{z}$. Let us relate the ball B_y^i to B_z^i: $z_0\in B_z^i$ if $y_0=z_0\in B_y^i$, an indicator of multivalued synchronization We can use the equality

$$\lim_{n\to\infty}|\mathbf{y}_n-\mathbf{z}_n|=0, \tag{27}$$

where $(\mathbf{x}_n,\mathbf{y}_n,\mathbf{z}_n)=\psi_k^n(\mathbf{x}_0,\mathbf{y}_0,\mathbf{z}_0)$ and $(\mathbf{x}_0,\mathbf{y}_0,\mathbf{z}_0)$, is an arbitrary point in B such that $y_0\in B_y^i$ and $z_0\in B_z^i$ with the same index i, as an indicator of multivalued synchronization. Indeed, it is simple to see that the following statement holds.

Theorem 5B. Under the assumptions of Theorem 1B the equality (27) is satisfied provided that $y_0\in B_y^i$ *and* $z_0\in B_z^i$ *with the same index i.*

The behavior of orbits in the attractor can be different. It could be related to a cyclic repetition, $h_1\to h_2\to h_1\to h_2\to\ldots$, or a more complex sequence of h_i. It depends on the partition of $\mathcal{A}_{k,x}$ into connected components.

In the simplest case when $\mathcal{A}_{k,x}$ is connected, every orbit in $\mathcal{A}_k$ behaves in the same way: for any i there is a j such that $\phi_k(graph(h_i))=graph(h_j)$, $1\leqslant i,j\leqslant p$. This fact is a direct corollary of Theorem 2B. Indeed, for any two points Q_1 and Q_2 in $graph(h_i)$ and any $\epsilon>0$ there is a collection of points $P_0,\ldots P_N\in graph(h_i)$ such that $P_0=Q_1$, $P_N=Q_2$ and dist$(P_i,P_{i+1})\leqslant\epsilon$, $0\leqslant i\leqslant N-1$. Because of the continuity of ϕ_k, the points $\phi_k(P_i)$ and $\phi_k(P_{i+1})$ belong to the same branch, say $g(h_j)$ for any $i=0,\ldots N-1$. In fact, a trajectory switches the disjoint balls in the y space in a particular order, and this order is uniquely determined by a permutation $i\to j$.

If $\mathcal{A}_{k,x}$ contains more than one connected components then the behavior of orbits inside each of them determines the same itinerary among branches $graph(h_i)$. For example, if such a component contains the projection of a periodic point then the itinerary will be also periodic. But if a component does not contain a periodic orbit then the itinerary could be nonperiodic; in this case $\mathcal{A}_{k,x}$ should have infinitely many connected components.

IV. CONCLUSIONS

The example of generalized synchronization of chaos considered in Sec. II enables us to explore properties of a type of chaos synchronization mapping in which the mapping is a multivalued function. Based on analysis of the conditional stability of the synchronous chaotic behavior of the response system, we come to conclusions concerning the existence and continuity of the synchronization mappings formed in these regimes of generalized synchronization. We used the auxiliary system method to detect the onset of conditional stability both in case of single-valued mappings and in case of multivalued mappings.

Changing the strength of the coupling between the drive and response systems, we followed the transition from a regime of synchronization with a single-valued function to a regime with a double-valued function. These two regimes of synchronization are separated by a regime of asynchronous chaotic oscillations. Our numerical analysis showed that this

regime of asynchronous oscillations occupies an interval of the coupling parameter values where all of the necessary bifurcations occur that are required for the formation of this type of synchronization mapping. Analysis of the unstable periodic orbits (UPOs) contained in the chaotic attractor formed in the joint phase space of drive and response systems revealed a very interesting element of this bifurcation scenario. We have found that not all UPOs in the attractor experience the period doubling bifurcations as the ribbon containing the chaotic trajectories of the attractor doubles its period. The UPOs with periods that are multiples to the period of the postbifurcation chaotic ribbon remain qualitatively unchanged. In this case the response system generates additional UPOs with identical periods via tangential bifurcations. Thanks to these additional UPOs the so formed double-valued synchronization function applies universally to all orbits of the driving chaotic attractor.

The introduction of multivalued synchronization mapping into the concept of the generalized synchronization of chaos provides another theoretical framework which is crucial for understanding of chaos synchronization phenomenon in many cases of synchronization in directionally coupled systems. Such cases include synchronization with frequency ratio other then 1:1 where the formation of multivalued synchronization mappings is a quite natural occurrence.

ACKNOWLEDGMENTS

The authors are grateful to H.D.I. Abarbanel, K. Josic, L. Kocarev, L. Pecora, and U. Parlitz for helpful discussions. N.F.R. was sponsored in part by U.S. Department of Energy (Grant No. DE-FG03-95ER14516) and the U.S. Army Research Office (MURI Grant No. DAAG55-98-1-0269).

[1] N. Minorsky, *Nonlinear Oscillations* (R. E. Krieger, Huntington, 1974), p. 714.
[2] I. I. Blekhman, Sinkhronizatsiia v prirode i tekhnike (Moskva: ''Nauka,'' Glav. red. fiziko-matematicheskoi lit-ry, Moscow, 1981), p. 351.
[3] L. Glass and and M. C. Mackey, *From Clocks to Chaos: The Rhythms of Life* (Princeton University Press, Princeton, 1988), p. 248.
[4] B. van der Pol, Philos. Mag. **3**, 65 (1927).
[5] V. Afraimovich, N. N. Verichev, and M. I. Rabinovich, Radiophys. Quantum Electron. **29**, 747 (1986).
[6] H. Fujisaka and T. Yamada, Prog. Theor. Phys. **69**, 32 (1984).
[7] L. M. Pecora and T. L. Carroll, Phys. Rev. Lett. **64**, 821 (1990).
[8] N. F. Rulkov, M. M. Sushchik, L. S. Tsimring, and H. D. I. Abarbanel, Phys. Rev. E **51**, 980 (1995).
[9] L. M. Pecora, T. M. Carroll, and J. F. Heagy, Phys. Rev. E **52**, 3420 (1995).
[10] L. Kocarev and U. Parlitz, Phys. Rev. Lett. **76**, 1816 (1996).
[11] S. J. Schift *et al.*, Phys. Rev. E **54**, 6708 (1996).
[12] A. Pikovsky *et al.*, Chaos **7**, 680 (1997).
[13] M. A. Zaks *et al.*, Phys. Rev. Lett. **82**, 4228 (1999).
[14] M. I. Rabinovich and H. D. I. Abarbanel, Neuroscience **87**, 5 (1998).
[15] R. Fitzgerald, Phys. Today **52**(3), 18 (1999); M. I. Rabinovich, Radiophys. Quantum Electron. **39**, 502 (1996).
[16] H. D. I. Abarbanel *et al.*, Usp. Fiz. Nauk **166**, 363 (1996) [Phys. Usp. **39**, 337 (1996)].
[17] B. R. Hunt, E. Ott, and J. A. Yorke, Phys. Rev. E **55**, 4029 (1997).
[18] K. Josic, Phys. Rev. Lett. **80**, 3053 (1998).
[19] V. Afraimovich, J.-R. Chazottes, and A. Cordonet, Discrete Continuous Dyn. Syst. B (to be published).
[20] N. F. Rulkov, Chaos **6**, 262 (1996).
[21] N. F. Rulkov and M. M. Sushchik, Int. J. Bifurcation Chaos **7**, 625 (1997).
[22] A. R. Volkovskii and N. F. Rulkov, Pis'ma Zh. Tekh. Fiz. **15**, 5 (1989) [Sov. Tech. Phys. Lett. **15**, 249 (1989)].
[23] H. D. I. Abarbanel, N. F. Rulkov, and M. M. Sushchik, Phys. Rev. E **53**, 4528 (1996).
[24] U. Parlitz, L. Junge, and L. Kocarev, Phys. Rev. Lett. **79**, 3158 (1997).
[25] N. F. Rulkov and M. M. Sushchik, Phys. Lett. A **214**, 145 (1996).
[26] E. H. Park, M. A. Zaks, and J. Kurths, Phys. Rev. E **60**, 6627 (1999).
[27] T. Sauer, C. Grebogi, and J. A. Yorke, Phys. Rev. Lett. **79**, 59 (1997).
[28] Ch. G. Schroer, E. Ott, and J. A. Yorke, Phys. Rev. Lett. **81**, 1397 (1998).
[29] E. Barreto and P. So, Phys. Rev. Lett. **85**, 2490 (2000).
[30] K. Pyragas, Phys. Rev. E **54**, R4508 (1996).